

AD-754 837

OXIDE CERAMIC LASER

Charles D. Greskovich

General Electric Corporate Research and  
Development

Prepared for:

Advanced Research Projects Agency  
Office of Naval Research

25 January 1973

DISTRIBUTED BY:

**NTIS**

National Technical Information Service  
U. S. DEPARTMENT OF COMMERCE  
5285 Port Royal Road, Springfield Va. 22151

AD 754837

## OXIDE CERAMIC LASER

SEMI-ANNUAL TECHNICAL REPORT (ITEM 0002-A002)

Program Code No.: 02D10K71  
Contract No.: N00014-70-C-0360  
Principal Investigator: Charles D. Greskovich  
(518) 346-8771  
Ext. 6122  
Contractor: General Electric Company  
Effective Date: June 1, 1970  
Expiration Date: May 31, 1973  
Amount of Contract: \$297,398.00  
January 25, 1973  
Scientific Officer: A. M. Diness, Code 471  
Office of Naval Research  
Arlington, Va. 22217

### Sponsored By

Advanced Research Projects Agency  
ARPA Order No. 1587, Amend. #3

The views and conclusions contained in this document are those of the author and should not be interpreted as necessarily representing the official policies, either expressed or implied, of the Advanced Research Projects Agency or the U. S. Government.

This research was supported by the Advanced Research Project Agency of the Department of Defense and was monitored by ONR under Contract No. N00014-70-C-0360.

Reproduced by  
NATIONAL TECHNICAL  
INFORMATION SERVICE  
U.S. Department of Commerce  
Springfield, VA 22151

UNCLASSIFIED

Security Classification

DOCUMENT CONTROL DATA - R & D

(Security classification of title, body of abstract and indexing annotation must be entered when the overall report is classified)

1. ORIGINATING ACTIVITY (Corporate author) General Electric Company Corporate Research & Development Post Office Box 8 Schenectady, New York 12301		2a. REPORT SECURITY CLASSIFICATION Unclassified	
3. REPORT TITLE OXIDE CERAMIC LASER		2b. GROUP	
4. DESCRIPTIVE NOTES (Type of report and inclusive dates) Semi-Annual Technical Report, January 25, 1973			
5. AUTHOR(S) (First name, middle initial, last name) Charles D. Greskovich			
6. REPORT DATE January 25, 1972	7a. TOTAL NO. OF PAGES 35 42	7b. NO. OF REFS 5	
8a. CONTRACT OR GRANT NO. N00014-70-C-0360	9a. ORIGINATOR'S REPORT NUMBER(S) SRD-73-017		
b. PROJECT NO. ARPA Order #1587 Amend. #3	9b. OTHER REPORT NO(S) (Any other numbers that may be assigned this report)		
c. 02D10K71	d.		
10. DISTRIBUTION STATEMENT Detail. of illustrations in this document may be better studied on microfiche.			
11. SUPPLEMENTARY NOTES		12. SPONSORING MILITARY ACTIVITY Advanced Research Projects Agency 1400 Wilson Boulevard Arlington, Virginia 22209	
13. ABSTRACT Several attempts were made to reduce or eliminate orange peel and extended defect formation in NDY ceramics by introducing changes in powder preparation, processing, and thermal cycling conditions. The preparation of oxalate powder by an aerosol technique reduced residual porosity and orange peel in sintered material made from unmilled powder. A dry milling operation was, nevertheless, the most effective method of reducing orange peel. The lasing performance of NDY laser rods is probably limited by submicroscopic scattering centers having compositional variations in the solid solution matrix. Evidence of substructure in the matrix was revealed by ultramicroscopy and chemical etching techniques. A rapid cooling treatment, again, produced a laser rod with improved lasing performance. It was discovered that controlled oxidation of Yttralox generates a pronounced IR filter behavior.			

DD FORM 1473

I-a

UNCLASSIFIED

Security Classification

UNCLASSIFIED

Security Classification

14 KEY WORDS	LINK A		LINK B		LINK C	
	ROLE	WT	ROLE	WT	ROLE	WT
Nd-doped Yttrium Oxide Lasers						
Transparent Polycrystalline Ceramics						
Submicroscopic Scattering Centers						
Sintering						
Pores						
Spectral Transmittance						

I-6

UNCLASSIFIED

Security Classification

## TABLE OF CONTENTS

	<u>Page No.</u>
TITLE PAGE-----	
FOREWORD -----	i
ABSTRACT -----	ii
LIST OF ILLUSTRATIONS -----	iii
I. INTRODUCTION -----	1
II. INFLUENCE OF POWDER PREPARATION AND PROCESSING ON ORANGE PEEL, POROSITY, AND SOLID SECOND PHASE-----	2
A. Experimental Procedures -----	2
B. Orange Peel-----	8
C. Residual Porosity and Solid Second Phase -----	13
III. ATTEMPTS TO IDENTIFY SUBMICROSCOPIC SCATTERING CENTERS -----	22
A. X-ray Diffraction Results -----	23
B. Electron Microscope Results -----	24
C. Ultramicroscopy -----	26
IV. OPTICAL MEASUREMENTS -----	29
A. Lasing Measurements -----	29
B. Laser Damage Threshold-----	33
C. Influence of Stoichiometry on Transparency of Yttrium Oxide -----	34
V. REFERENCES -----	34

I-C

## FOREWORD

This research was sponsored by Advanced Research Projects Agency and carried out in the Metallurgy and Ceramics Laboratory and the General Physics Laboratory of the General Electric Company Corporate Research and Development under U.S. Navy Contract N00014-70-C-0360 entitled "Oxide Ceramic Laser".

This work was administered under the direction of Dr. Arthur Diness from June 1, 1971, to May 31, 1973.

The author acknowledges the contributions of the following individuals to the Program:

- R. J. Charles, for helpful guidance during this program:
- J. C. Almasi and J. P. Chernoch, for active and passive optical measurements:
- C. O'Clair, for ceramic processing procedures and heat treatments.

LIST OF ILLUSTRATIONS

<u>Figure No.</u>		<u>Page No.</u>
1	SEM photomicrograph of NDY oxalate powder prepared by the standard oxalate method, X5,000	5
2	SEM photomicrograph of NDY oxalate powder prepared by dripping hot nitrate solutions into cold oxalic acid solution, X5,000 -----	6
3	SEM photomicrograph of (a) NDY oxalate powder prepared by the aerosol technique, (X5,000) and (b) same powder calcined for 4 hours at 850°C, X10,000 -----	7
4	Substructure in sintered NDY ceramic prepared from oxalate powder made by pouring the Y-Th-Nd salt solution into the oxalic acid solution. Sintering treatment 8 hours at 2000°C. Chemically-etched for 1 min. in 1 part H <sub>2</sub> O and 1 part HCl (boiling, X500 -----	11
5	Substructure in sintered NDY ceramic prepared from milled calcined powder derived from the standard oxalate method. Sintering treatment 38 hours at 2170°C, fast-cooled to room temperature. Chemically-etched for 1.5 min. in boiling 1 part H <sub>2</sub> O + 1 part HCl, X500	12
6	Pore density versus pore size in NDY rod (13-7) sintered for 60 hours at 2170°C. Specimen made from unmilled calcined oxalate powder derived from the standard drip method -----	14
7	Pore density versus pore size in NDY ceramic (26-1). Sintered for 40 hours at 2170°C. Specimen made from unmilled calcined oxalate powder derived from the aerosol technique -----	15
8	High pore density observed in NDY ceramic prepared from oxalate powder derived from dripping cold Y-Th-Nd nitrate solution into hot oxalic acid solution. Sintering treatment 40 hours at 2170°C. Transmitted light, X374 -----	17
9	Pore density versus pore size in NDY ceramic made by the aerosol technique and sintered for 40 hours at 2170°C. (a) unmilled powder and (b) milled oxalate powder -	18

<u>Figure No.</u>		<u>Page No.</u>
10	Porous, second phase inclusion in NDY ceramic prepared from unmilled powder. Transmitted light. X440 -----	20
11	Porous, second phase inclusion in NDY ceramic prepared from unmilled powder. Polarized light using crossed nicols, X440-----	21
12	Electron transmission photomicrograph of grain boundaries NDY ceramic thinned by ion micro-milling, X48,000 -----	25
13	Ultramicroscope photomicrograph of scattering centers in a NDY ceramic rod, X10 -----	27
14	Effect of output mirror reflectivity ( $R_2$ ) on the pump energy required for laser threshold. Same rod that was fast-cooled (12-1A) and slow-cooled (12-1B) from the sintering temperature of 2170°C. $R_1 \approx 1$	31
15	Energy output versus energy input for the same rod that was fast-cooled (12-1A) and slow-cooled (12-1B) from the sintering temperature of 2170°C, laser glass (OI - ED-2) was used as a reference material-----	32



## I. INTRODUCTION

The long-range goal of the current program is to develop an intermediate gain solid laser host material which exhibits a behavior between that of neodymium-doped glass and yttrium aluminum garnet single crystal; i.e., suitable for generating high average power combined with high peak power. In order to achieve this goal, experimental and theoretical work has been done and is currently in progress to (1) develop improved powder preparation and processing procedures to reproducibly fabricate Yttralox<sup>TM</sup> (composed of a solid solution of 89 mole %  $Y_2O_3$ , 10%  $ThO_2$  and 1%  $Nd_2O_3$ ) with improved optical quality, (2) understand the development of the microstructure and the densification process with respect to the kinetics of porosity and grain size changes, and (3) evaluate neodymium-doped and neodymium-free Yttralox ceramic as a potential high-power intermediate gain laser and as a high-power infrared window material, respectively by means of optical measurements.

In a recent Annual Technical Report,<sup>1</sup> it was pointed out that one or more scattering mechanisms appears to be responsible for much of the attenuation of laser radiation in neodymium-doped Yttralox (NDY) rods. Furthermore, it was deduced that submicroscopic scattering centers most likely exist in NDY laser rods because (1) preliminary light scattering calculations showed that the observed porosity cannot account for the high scattering losses and (2) the active attenuation coefficient measured from lasing performance data was influenced by the cooling cycle imposed on a laser rod. By a fast cooling technique, for example, the active attenuation coefficient for one rod was reduced from about 4.9%/cm to 2.6%/cm.

In the past six months, the current research program was directed in such a way as to attempt to minimize the formation of submicroscopic scattering centers by assuming their most probable origin. In addition, various experimental methods and tools were employed to attempt to detect such scattering centers. There were two main plans of attack. It was assumed that the most reasonable origins of submicroscopic scattering centers responsible for the high scattering losses observed in NDY ceramic was "orange peel" effects and/or extended defects which form in the solid solution matrix

---

TM = General Electric Trademark

during the cooling cycle. The orange peel problem involved attempts to minimize chemical inhomogeneities in the starting powder by improved powder preparation and processing techniques; extended firing times at high temperatures has not been very effective in appreciably reducing orange peel. A rapid cooling technique is currently being employed to retard the nucleation and growth of extended defects because a second NDY laser rod prepared by utilizing the rapid cooling process also showed improved lasing performance when compared to that obtained from the same specimen having a slow cooling treatment. Many of the experimental results and problems encountered during this investigation of methods to reduce or eliminate orange peel and extended defects will be described for the solid solution material, Yttralox.

## II. INFLUENCE OF POWDER PREPARATION AND PROCESSING ON ORANGE PEEL, POROSITY, AND SOLID SECOND PHASE

### A. Experimental Procedures

The oxalate precipitation method<sup>1</sup> is an excellent source of high-purity, fine-particle size (0.3 to 3  $\mu\text{m}$ ) oxalate powder which has physical and chemical properties that are favorable for a sintering approach. Unfortunately, sintered NDY ceramic prepared from unmilled calcined powder produced by the oxalate process contains "orange peel", a point-to-point variation in refractive index throughout the material volume. Orange peel is thought to be related to chemical inhomogeneities ( $\text{Th}^{4+}/\text{Y}^{3+}$  ratio differences) formed in various regions of the oxalate precipitate during powder preparation. This reasoning is supported by the fact that orange peel is reduced by screening or ball-milling the calcined powder before powder compaction. Both processing steps have a tendency to reduce compositional variations on a large scale in the starting powder, thereby promoting a faster approach to chemical equilibrium by interdiffusional processes during sintering at high temperatures.

Attempts were made to develop an improved powder preparation and processing procedure to reproducibly fabricate Yttralox ceramic with reduced orange peel. It was decided to make several changes in the oxalate precipitation method and subsequent processing steps in order to more thoroughly explore this method. Before describing these changes, the standard oxalate process will be described for a comparative analysis.

The standard oxalate process involves the dripping of a salt solution of an yttrium, thorium, and neodymium nitrates, in the proper proportion to yield a composition 89 mole %  $Y_2O_3$ , 10%  $ThO_2$ , and 1%  $Nd_2O_3$ , at a rate of about 60 drops/min. into an oxalic acid bath which was 80% saturated at room temperature and contained 100% excess oxalic acid required to convert the nitrates into oxalates. During precipitation at room temperature, the oxalic acid bath is continuously stirred with a Teflon-coated, magnetic stirring bar. After precipitation, the oxalate precipitate is washed with filtered deionized water to remove residual acid, vacuum-filtered, dehydrated at 110°C for 24 hours, and calcined for four hours at 850°C in flowing air (3SCFH). The calcined powder can be either directly cold-pressed into shape or dry-milled with 1 wt. % stearic acid in a rubber-lined ball mill (Vol. = 1.2ℓ) that contains  $ThO_2$ -doped  $Y_2O_3$  cylinders as a grinding medium. After ball-milling for six hours, specimens are formed into shape by isostatic pressing between 20,000 and 40,000 psi, given an oxidation treatment in air at 1100°C for two hours, sintered in dry  $H_2$  (dew point  $\sim 70^\circ C$ ) at 2170°C for 30 to 100 hours, and finally cooled to room temperature in about six hours in wet  $H_2$  (dew point  $\sim 25^\circ C$ ).

An investigation was made to see if chemical segregation and particle size and morphology could be influenced by the temperature of oxalate precipitation. Two experimental changes introduced in the drip method of oxalate powder preparation were (1) to drip hot (85°C) nitrate salt solution into a cold (5°C) oxalic acid bath, and (2) to drip cold (5°C) nitrate salt solution into a hot (90°C) oxalic acid bath.

An aerosol technique was also developed to decrease the droplet size of the Y-Th-Nd salt solution from the millimeter size range (drip method) to the micron size range so that a chemically homogeneous and fine particle size powder would result. In this case, a brass aspirator was constructed such that a high-velocity air stream passed between a .003-inch diameter glass capillary (containing the nitrate salt solution) and a .040-inch diameter hole bored in a stainless steel disk used as an insert. The air flow was about 60 SCFH through this gap and all experiments were carried out at room temperature. One experiment involved the positioning the tip of the glass capillary about four inches above the surface of the stirred oxalic acid

bath. Unless the aerosol was enclosed in a large flask, airborne nitrate droplets were found condensed on the experimental apparatus as well as on the walls, windows, and bench top in the working hood. A second experiment was made by placing the tip of the glass capillary below the surface of the stirred oxalic acid bath. Here, a considerable amount of back pressure developed at the capillary tip, causing air bubbles to feed back through the capillary into the reservoir of salt solution. This problem could be largely overcome by repositioning of the capillary tip and by adjusting the air flow. Again, a white condensate appeared on the top inner surface of the glass flask containing the oxalic acid solution.

After stirring the resulting oxalate precipitate synthesized by the experiments described above, the settling behavior of the oxalate particles was not appreciably different than that observed in the standard drip method at room temperature. The one exception to this rule was found for the case of oxalate particles formed by dripping the cold salt solution into the hot oxalic acid bath. It was observed that the precipitate particles did not settle to a uniform depth, as is the usual observation, but piled high in the center of the beaker. Furthermore, the oxalate precipitate particles felt gritty, like sand, when rubbed between the fingers.

Particle morphology and size were studied by scanning electron microscopy (SEM). Figures 1, 2, and 3a illustrate oxalate particles derived from several methods of powder preparation. In all cases, the oxalate particles are approximately parallelepipeds or plates with a size range between about 0.3 and 3  $\mu\text{m}$ . Variations in powder preparation on the oxalate approach yielded similar particle sizes and shapes except for the exception described above. The state of agglomeration of the oxalate particles may at first appear to be different for the various powder preparation techniques but dispersing and settling effects introduced during specimen preparation for the SEM may partly be responsible for this observation. Figure 3b is a typical scanning electron micrograph of calcined oxalate powder prepared by dripping the hot nitrate salt solution into the cold oxalic acid bath. Powder agglomerates are no doubt present after calcination at 850°C for four hours.



Fig. 1 SEM photomicrograph of NDY  
oxalate powder prepared by the standard  
oxalate method. 5,000X



Fig.2 SEM photomicrograph of NDY oxalate powder prepared by dripping hot nitrate solutions into cold oxalic acid solution. 5,000X



(a) 5,000X



(b)

Fig. 3 SEM photomicrograph of  
(a) NDY oxalate powder prepared by the aerosol technique  
(b) same powder calcined for 4 hours at 850°C. 10,000X

Oxalate precipitate particles synthesized by dripping the cold nitrate salt solution into the hot oxalic acid bath were as large as a millimeter in size but after dehydration at 110°C for 12 hours, these coarse particles disintegrated into micron-sized particles. It is believed that under the experimental conditions, the hot oxalic acid bath permits excess water of crystallization to be incorporated into the "oxalate-hydrate" particles and permits the growth of large aggregates. Upon dehydration at 110°C, the excess water of crystallization is eliminated to form a more stable form of the oxalate-hydrate. An extensive investigation of this powder was not done because this powder produced sintered material having a considerable degree of orange peel, porosity, and solid second phase.

One major processing change introduced in the oxalate process was the dry-milling of the oxalate powder in the presence of 1 wt. % stearic acid before the calcination step, not after it. If this processing step helped to improve the optical quality; i.e., reduce residual orange peel, porosity, and solid second phase of sintered NDY ceramic above that produced by the usual processing sequence, then it would be possible to eliminate the oxidation treatment as a processing step. The consequences of this change in powder processing is described in the subsequent sections.

#### B. Orange Peel

The amount of orange peel in NDY ceramic is qualitatively evidenced by the detection of an optical waviness inside of a polished specimen with the unaided eye and by a "grainy texture" observed by viewing the specimen slightly out of focus at low magnifications ( $\approx X60$ ) with the optical microscope using a pinhole source of transmitted white light. For comparative analyses, both methods for detection of orange peel give essentially the same result. A quantitative definition of orange peel in NDY ceramics will be obtained by the interpretation of optical interference patterns and is already in progress.

In comparison to the amount of orange peel found in sintered material prepared from unmilled powder produced by the conventional drip method, less orange peel was observed when the oxalate precipitate was produced by the aerosol technique or when the hot nitrate salt solution was



dripped into the cold oxalic acid solution. If orange peel resulted from selective precipitation of yttrium- and thorium-rich oxalate particles, then a decreased size of the nitrate droplets or an increased surface area of these droplets favor a higher reaction rate with the oxalic acid to form oxalate particles of more uniform composition and/or form a smaller average particle size which promotes a better dispersion of the two major components. In either case, the  $Y^{3+}/Th^{4+}$  ratio is reduced to a finer scale. The drip method used for adding hot nitrate solution into cold oxalic acid apparently achieves a similar result. It may be that chemical inhomogeneities may be reduced for this method because the viscosity of the nitrate solution is reduced enough to increase the flux of yttrium and thorium ionic complexes reaching the interface between the nitrate droplet and the oxalic acid solution. The aerosol technique, although more difficult to control, gave rise to sintered material with less orange peel than that produced by the drip method (hot nitrate into cold oxalic acid). However, the drip method (cold nitrate into hot oxalic acid) gave rise to sintered material exhibiting an unusually large amount of orange peel.

Orange peel can be reduced markedly by dry-ball-milling oxalate powders derived by any of the powder preparation methods described above. It is found that ball-milling the oxalate powder in the presence of 1 wt. % stearic acid before or after the calcination step gives rise to sintered material with the best optical quality. Ball milling reduces the size of the particles, mixes and disperses yttrium-rich and thorium-rich regions more homogeneously throughout the starting powder, and comminutes powder agglomerates that could result in compositional inhomogeneities and large pores in the sintered product.

Additional evidence of orange peel in sintered NDY ceramic was obtained by chemically etching a well-polished surface with boiling 1 part HCl + 1 part H<sub>2</sub>O for 1 to 1.5 minutes. The amount of orange peel in NDY ceramic was exaggerated to reveal subtle differences in the etching behavior of different regions within the grains. Orange peel was exaggerated by synthesizing a starting oxalate powder by a method in which the Y-Th-Nd salt solution was poured slowly into a vigorously stirred oxalic acid solution. A chemically etched, polished section of the sintered material

made from unmilled powder is shown in Fig. 4. Note that a substructure is clearly revealed in most grains in this specimen having an average grain size of 10  $\mu\text{m}$ . Closer examination of the microstructure at magnifications up to X1000 showed that virtually all grains contained substructure. The revelation of substructure was more apparent in some grains than in others and may be related to the effect of grain orientation on chemical etching.

The substructure within the grains is characterized by irregularly shaped regions up to about 5  $\mu\text{m}$  in size which, in several instances, appear to interconnect from one grain to another without any regard for the grain boundary. Apparently, these grains have nearly the same crystallographic orientation and chemically-etch at about the same rate so as to reveal this substructural appearance. On this basis, it seems that the origin of the substructure occurred very early in the development of the microstructure and is probably related to the presence of chemical inhomogeneities in the starting powder. In many cases, nearly spherical regions about 1 or 2  $\mu\text{m}$  in size are observed inside grains and could be the remnants of the original powder particles having variable composition. It is suggested that rapid grain growth took place during the early stages of sintering and left behind the trails caused by chemical segregation. These small compositional or impurity differences do not disappear even after prolonged firing times at temperatures near 90% of the melting point. For example, Figure 5 shows a chemically-etched microstructure of an Yttralox sample which was prepared from a milled powder, sintered for 38 hours at 2170°C, and then cooled rapidly to room temperature. Specimens cooled slowly to room temperature give rise to the same type of microstructure. The substructure is again pronounced in some grains but there is not as much coarseness to the substructure as was evident in Fig. 4. It appears that the coarseness of the substructure is related directly to orange peel which is caused by chemical segregation of yttria and thoria in the starting powder. The substructure is not composed of low angle grain boundaries, or subgrains, because electron transmission and diffraction results showed no evidence of dislocation networks outlining subgrain boundaries or of any detectable difference in crystallographic orientation with position inside a grain.

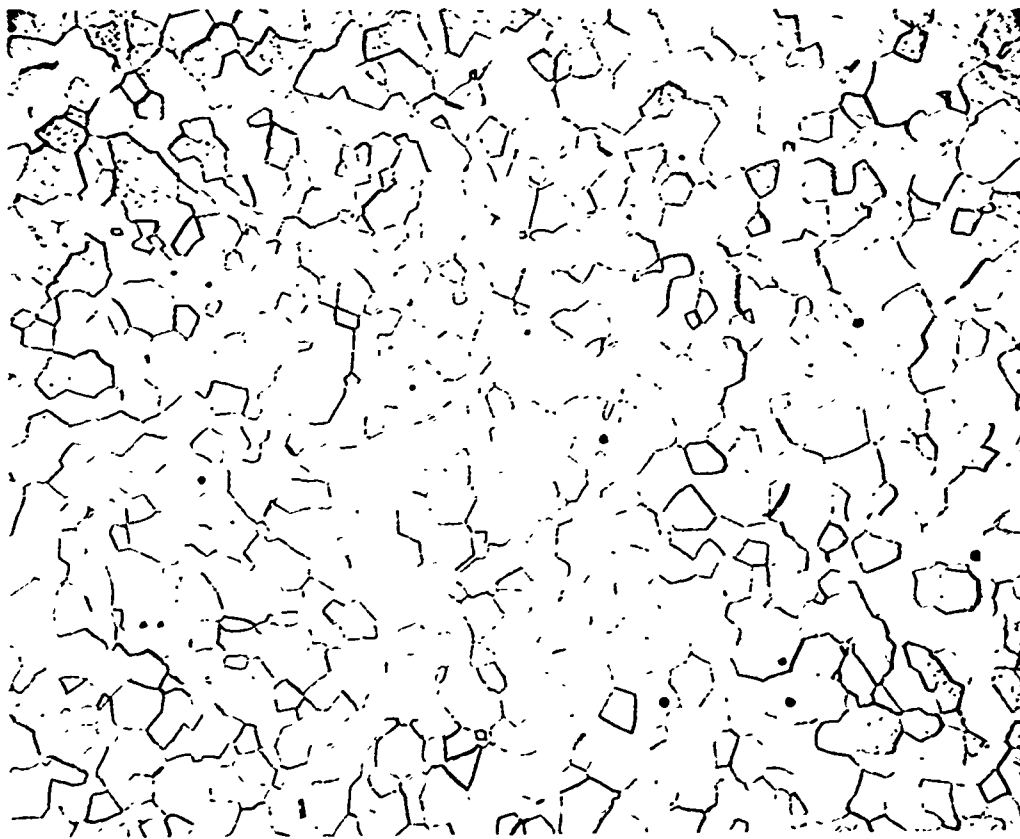


Fig.4 Substructure in sintered NDY ceramic prepared from oxalate powder made by pouring the Y-Th-Nd salt solution into the oxalic acid solution. Sintering treatment, 8 hours at 2000°C. Chemically-etched for 1 minute in 1 part H<sub>2</sub>O and 1 part HCl (Boiling). 500X

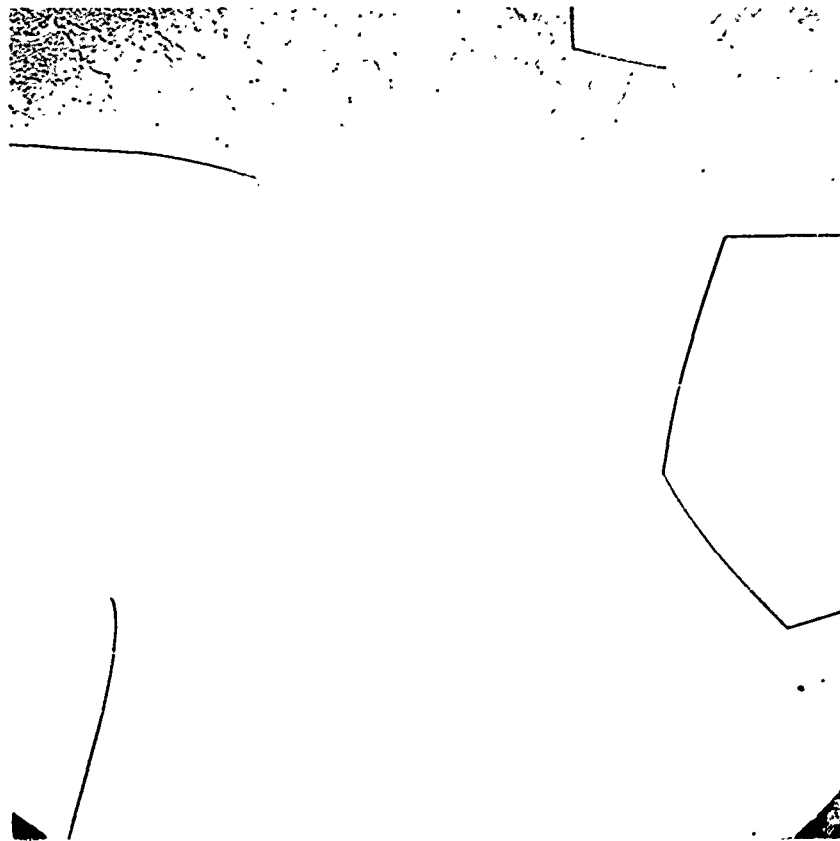


Fig. 5 Substructure in sintered NDY ceramic prepared from milled calcined powder derived from the standard oxalate method. Sintering treatment 38 hours at 2170°C, fast-cooled to room temperature chemically-etched for 1.5 min. in boiling 1 part H<sub>2</sub>O + 1 part HCl. 500X

### C. Residual Porosity and Solid Second Phase

If NDY ceramic is made from unmilled calcined oxalate powder derived by the conventional drip technique at room temperature, material sintered for about 60 hours at 2170°C contains approximately  $3.5 \times 10^{-5}$  porosity and no solid second phase. The majority of pores have sizes between 0.5 and 5  $\mu\text{m}$  and are distributed randomly throughout the specimen (Fig. 6). Between  $10^4$  and  $10^5$  pores/cm<sup>3</sup> are found for 0.6  $\mu\text{m}$  intervals for pore sizes <5  $\mu\text{m}$ . In addition, pore density decreases with pore size as expected; but an occasional pore as large as 200  $\mu\text{m}$  (not indicated on the frequency curve) can be observed in these sintered specimens. In several cases, a few isolated pore clusters are visible under transmitted light.

Pore density as a function of pore size is illustrated in Fig. 7 for sintered material prepared from oxalate powder derived by the aerosol technique. Again, the majority of pores have sizes between 0.5 and 5  $\mu\text{m}$  and appear to be randomly distributed, except in a few cases. Between  $10^3$  and  $10^4$  pores/cm<sup>3</sup> are observed for 0.6  $\mu\text{m}$  intervals for pore sizes <5  $\mu\text{m}$ . A comparison of the total pore density between 0.5 and 5  $\mu\text{m}$  found in sintered material made by the standard drip method and the aerosol technique shows that the latter material has more than two orders of magnitude fewer pores in this pore size range and also fewer larger pores. Large pores contribute greatly to pore volume and, as a result, the residual porosity in sintered material made by the aerosol technique ( $1.7 \times 10^{-5}$ ) is only about a factor of 2 lower than that found in material derived by the standard drip method.

Most small pores less than 10  $\mu\text{m}$  in size are located usually inside grains in these large grain-size ceramics. The entrapment of pores inside growing grains is strong evidence of ineffective inhibition of rapid grain growth. It has been previously demonstrated<sup>2</sup> that the addition of 10 mole % ThO<sub>2</sub> to Y<sub>2</sub>O<sub>3</sub> inhibits discontinuous grain growth during densification, thereby permitting most pores to remain on grain boundaries and eventually to shrink and disappear. A high level of pore elimination is predicted when the ThO<sub>2</sub> has a small particle size ( $\approx 1 \mu\text{m}$ ) and is uniformly dispersed throughout the starting calcined powder and/or the ThO<sub>2</sub> is completely dissolved in the small Y<sub>2</sub>O<sub>3</sub> particles. The aerosol technique of synthesizing the oxal powder apparently achieves an excellent dispersion of ThO<sub>2</sub> in the

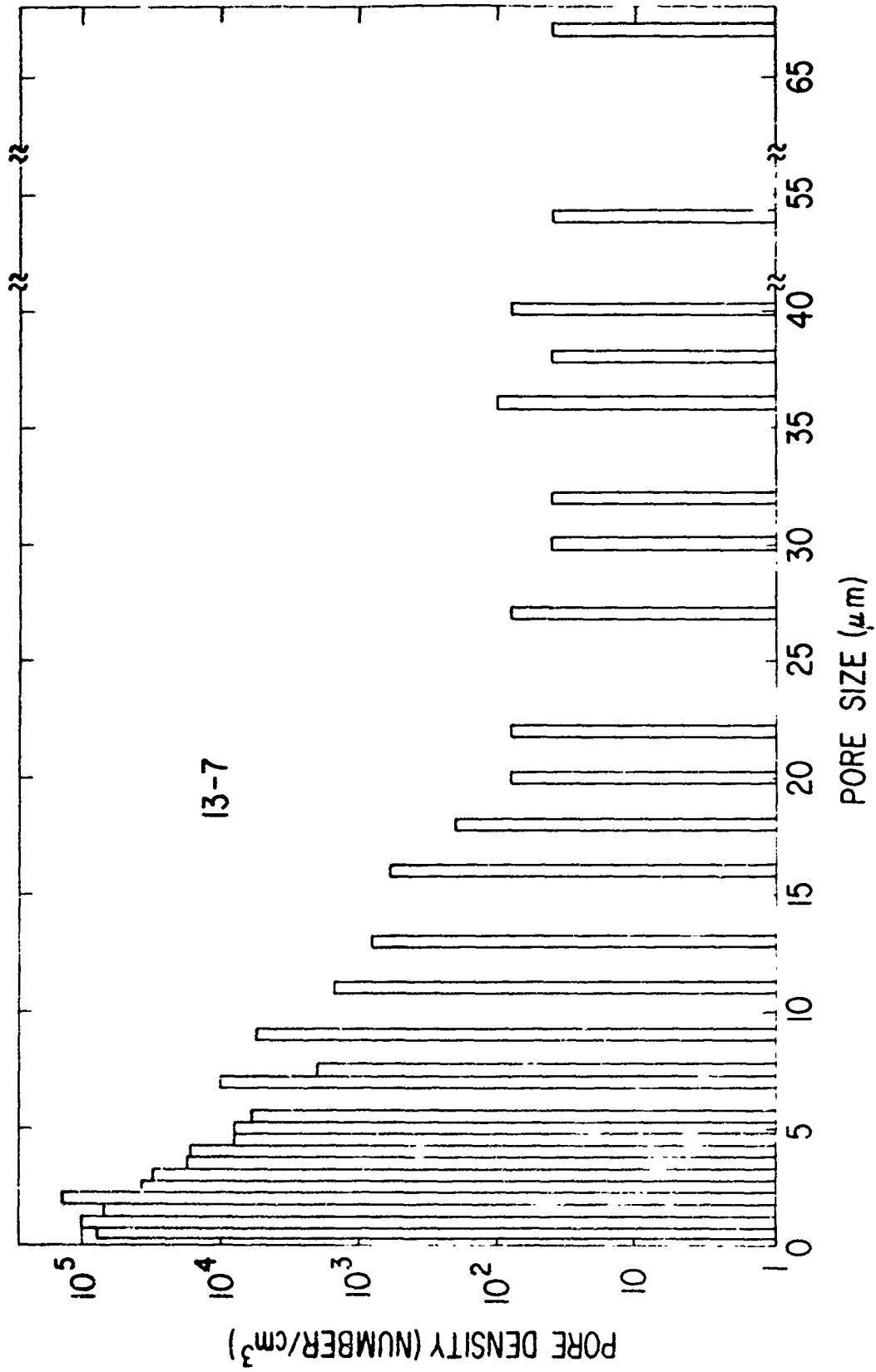


Fig. 6 Pore density versus pore size in NDY rod (13-7) sintered for 60 hours at 2170°C. Specimen made from unmilled calcined oxalate powder derived from the standard drip method.

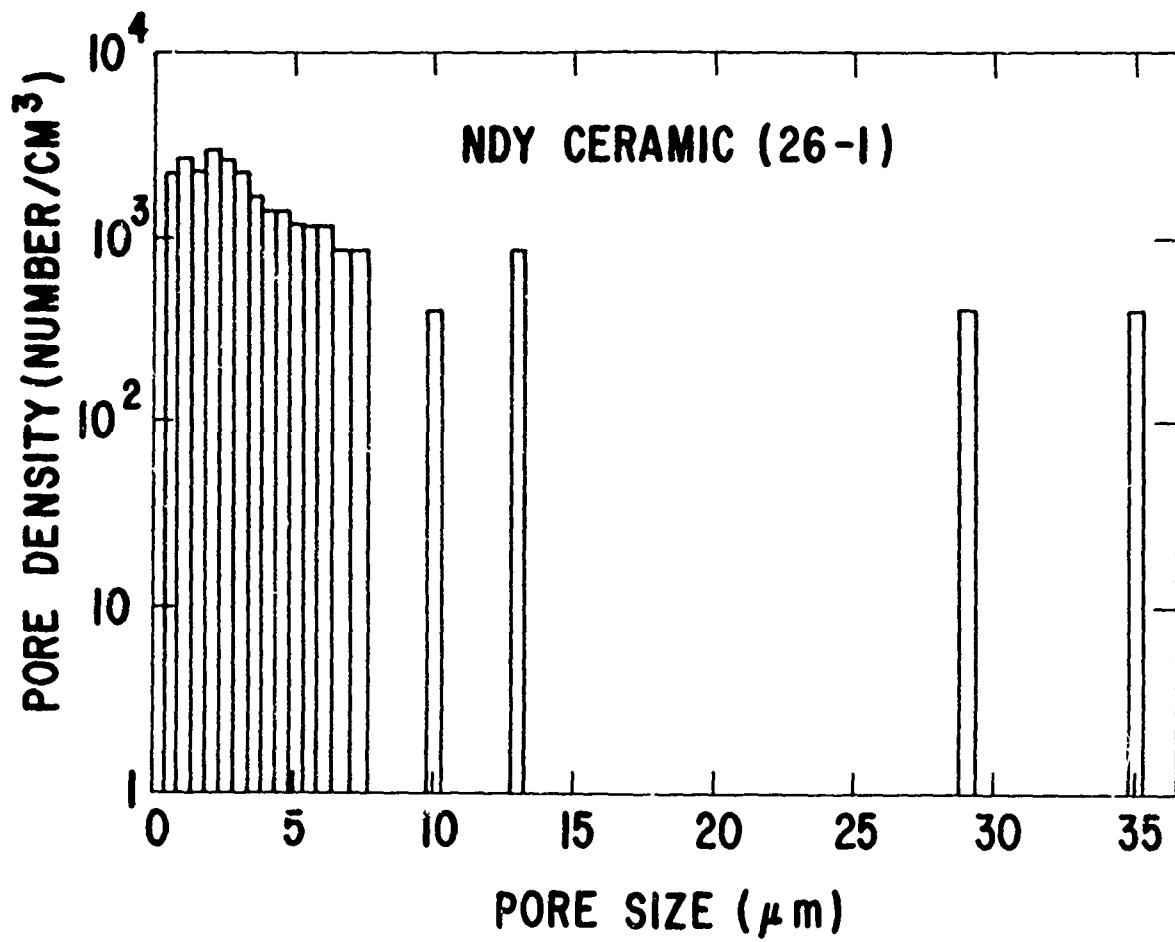


Fig. 7 Pore density versus pore size in NDY ceramic (26-1). Sintered for 40 hours at 2170°C. Specimen made from unmilled calcined oxalate powder derived from the aerosol technique.

starting powder so that the average grain boundary mobility is reduced during the early stages of grain growth.

Oxalate powder derived by the addition of hot nitrate salt solution into the cold oxalic acid solution also gave rise to sintered material containing lower pore densities for pores less than 5  $\mu\text{m}$  in size than that prepared from the standard drip method but not quite as low as that prepared by the aerosol technique. Oxalate powder derived by the addition of cold nitrate solution into hot oxalic acid solution produced sintered material containing unusually high pore densities for pores less than 5  $\mu\text{m}$  in size and also a high density of pore clusters (Fig. 8). A complex oxalate-hydrate reaction during oxalate precipitation created millimeter size agglomerates, as described above, and the high pore densities and large amount of orange peel associated with the resulting sintered material suggests that there is a large amount of chemical inhomogeneities in this starting powder.

It has been generally found that by ball-milling calcined oxalate powder in a rubber-lined mill, the pore density for a given pore size in sintered material is smaller than if the calcined powder received no milling treatment. Many of the large pores found in sintered material made from milled powder were thought to originate from rubber particles initially incorporated into the powder compact; i.e., the sequence of processing steps were oxalate powder, calcination, ball-milling oxide powder, powder compaction, oxidation treatment, and sintering. A way to eliminate large pores created by the presence of rubber particles in the powder compact was to ball-mill the oxalate powder and then calcine it to decompose the rubber particles. This experiment was carried out for oxalate powder derived by the aerosol technique. There were no observable irregularities in the milled powder; but after calcination, much of the powder was in the form of spherical agglomerates, some of which did not disintegrate completely when squeezed between the fingers. Pore frequencies are compared in Fig. 9 for sintered material made from unmilled and milled powder. Sintered material made from milled oxalate powder contained approximately 20% fewer pores for pore sizes less than 6  $\mu\text{m}$  but, surprisingly, contained about 60% more pores



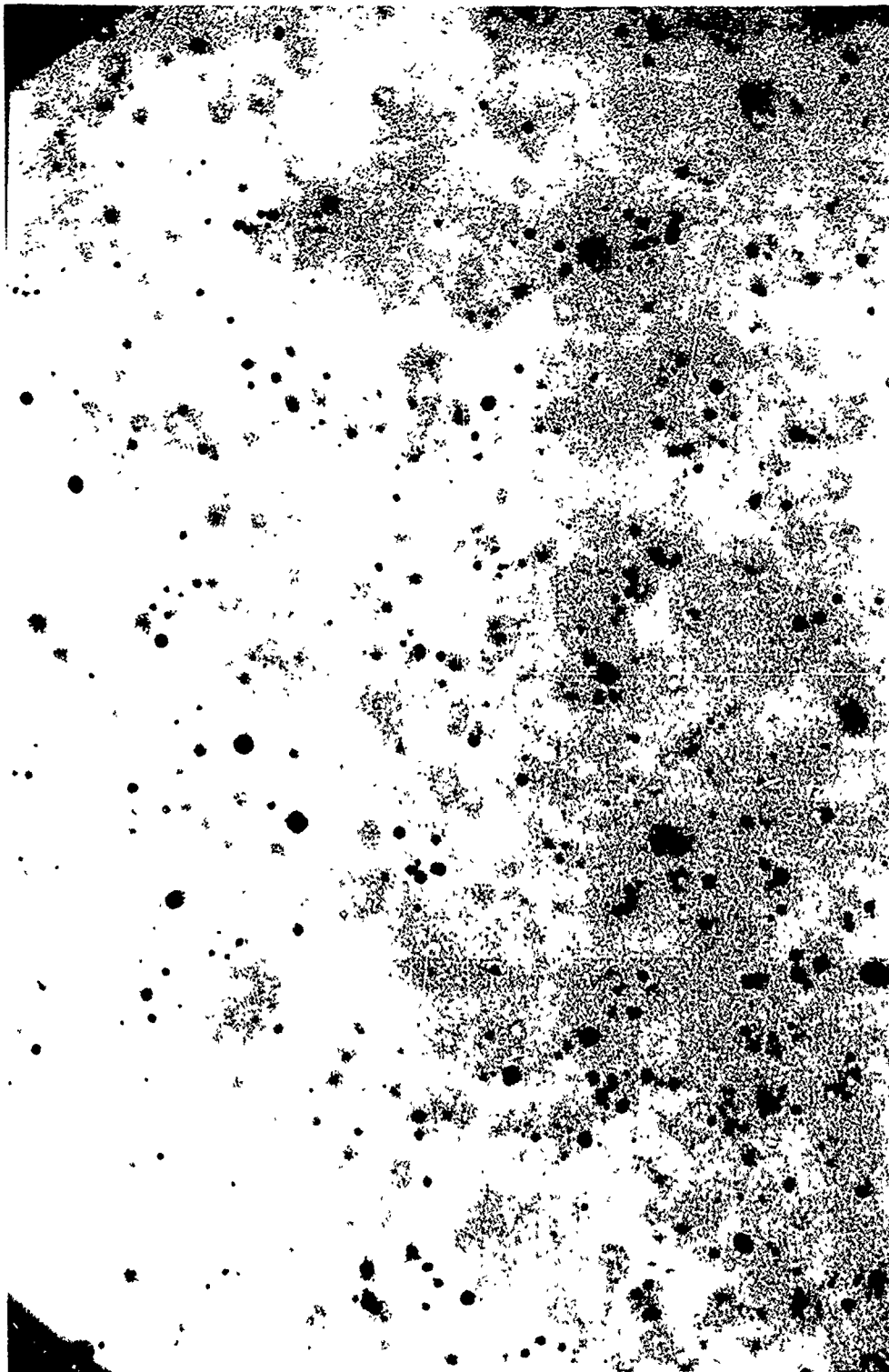


Fig. 8 High pore density observed in NDY ceramic prepared from oxalate powder derived from dripping cold Y-Th-Nd nitrate solution into hot oxalic acid solution. Sintering treatment 40 hours at 2170°C. Transmitted light. 374X

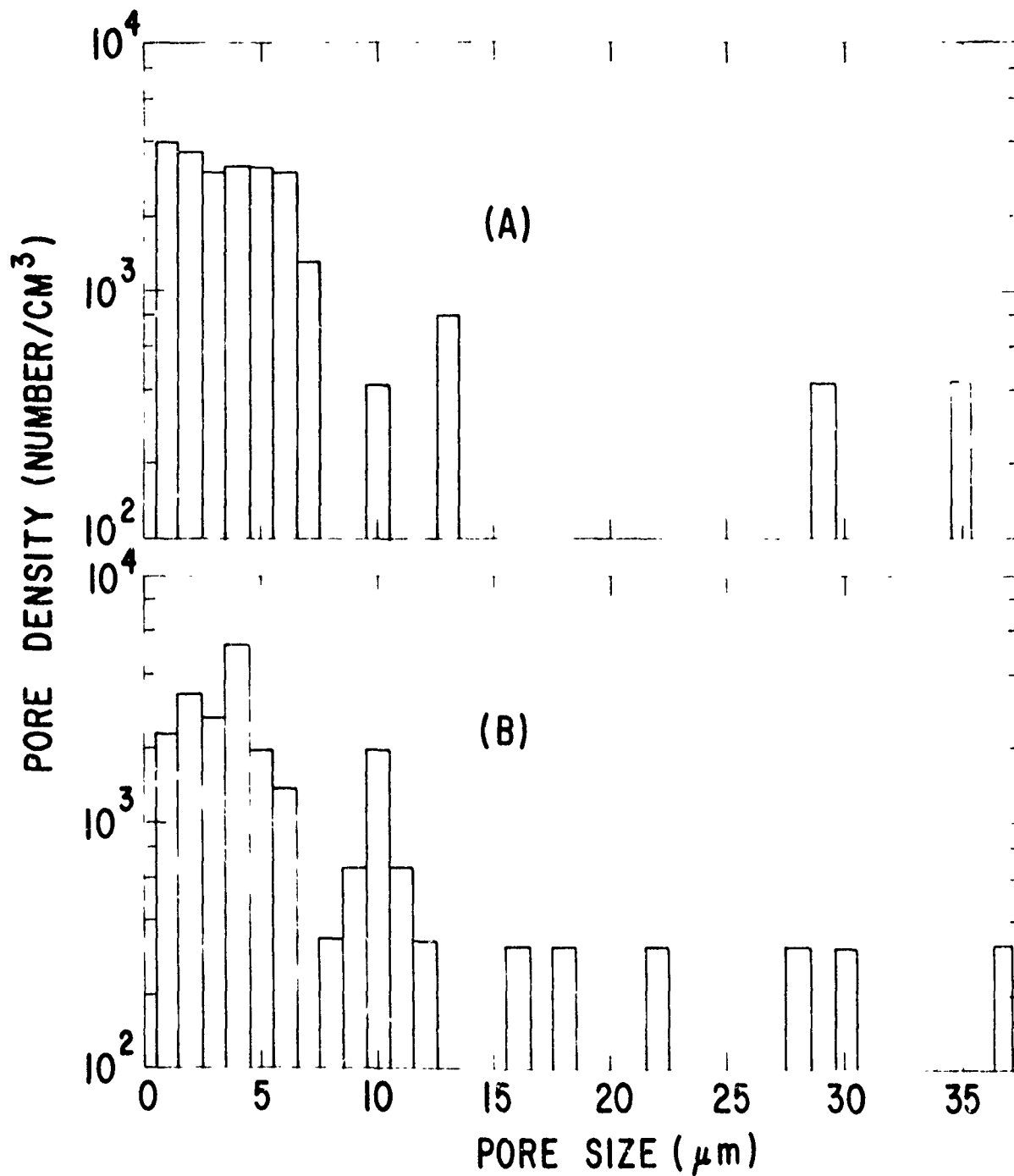


Fig. 9 Pore density versus pore size in NDY ceramic made by the aerosol technique and sintered for 40 hours at 2170°C. (a) unmilled powder and (b) milled oxalate powder.

greater than 6  $\mu\text{m}$ . In fact, the porosity in sintered material made from milled powder was about three times higher than that made from unmilled powder. The appearance of a bimodal distribution in Fig. 9B in which there is an additional peak in the pore density frequency curve at 10  $\mu\text{m}$  suggested that these pores originated probably from "hard" agglomerates which may or may not have a porous core. If the agglomerates were highly dense, then the formation of pores approximately 10  $\mu\text{m}$  in size may have resulted from microstructural inhomogeneities consisting of large pores created by the bridging of agglomerates or from differential shrinkage rates between particles located in a dense agglomerate and those in a more porous matrix.

A small number density of solid second phase particles were observed by transmitted light microscopy in sintered material made from unmilled powder produced by the aerosol technique. In sintered material produced by dripping hot nitrate solution into cold oxalic acid solution, no solid second phase inclusions could be observed at magnification as high as X625. A typical transmitted light photomicrograph of a second phase inclusion containing a considerable amount of porosity is shown in Figure 10. The large porous inclusion, about 60  $\mu\text{m}$  in size, was in fact polycrystalline because grain boundaries could be observed at the particle/matrix interface. Sintered material prepared by the aerosol technique contained, on the average, about 1 solid second phase particle per  $\text{mm}^3$  which ranged in size from 5 to 100  $\mu\text{m}$ . By using the Becke line method, the refractive index of the second phase particles was determined to be higher than that of the Yttralox matrix (R.I.  $\approx$  1.92 at the Na wavelength). The second phase particle is believed to be thoria-rich because pure  $\text{ThO}_2$  has a refractive index  $\approx$  2.2 at the sodium wavelength. Further evidence that the second phase particle has a composition largely different than that of the matrix can be obtained by observing the same particle as shown in Fig. 10 but with crossed polarizing elements (Fig. 11). Note that there is a strain field surrounding the particle which reveals many grain boundaries of the matrix phase. Stresses generating this strain are most likely caused by thermal expansion differences between the inclusion and matrix phases.



Fig. 10 Porous, second phase inclusion in NDY ceramic prepared from un-  
milled powder. Transmitted light.

440X

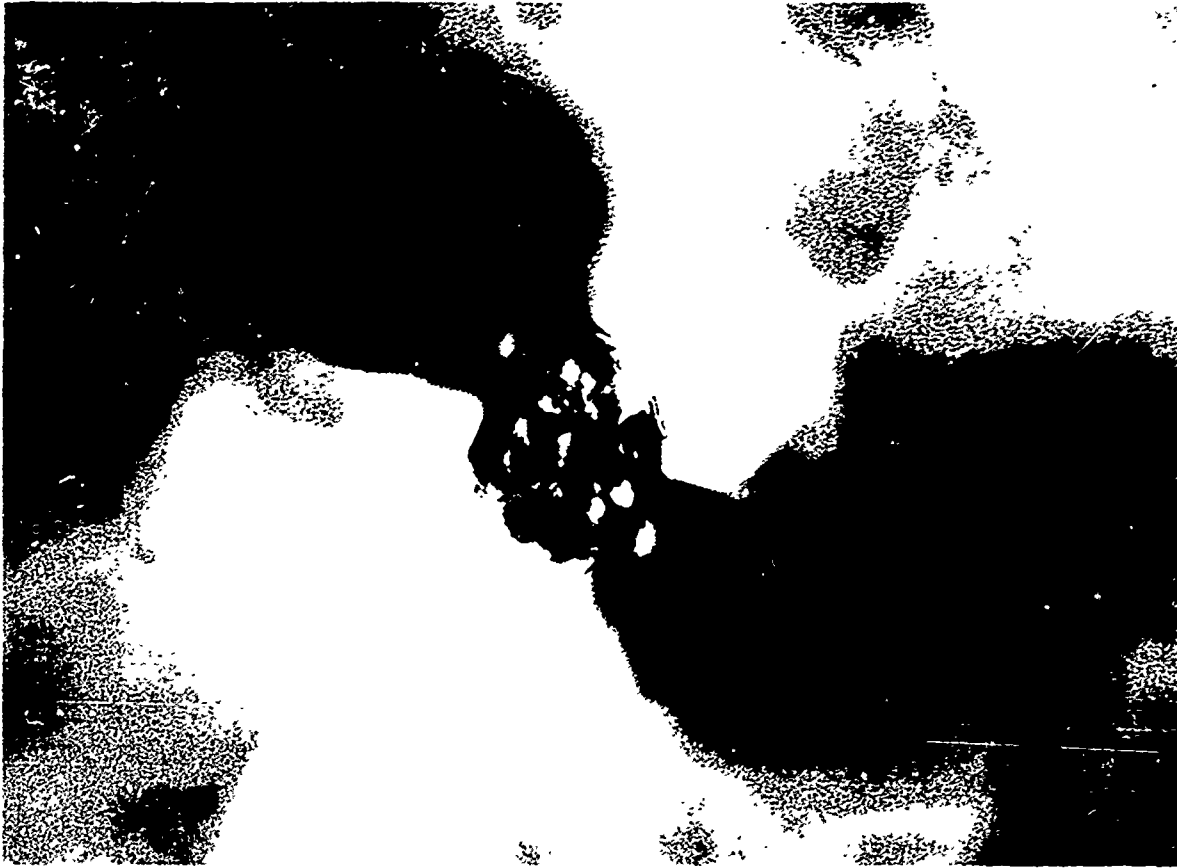



Fig. 11 Porous, second phase inclusion in NDY ceramic prepared from unmilled powder. Polarized light using crossed nicols. 440X

Reproduced from  
best available copy. 

The origin and elimination of second phase particles is of utmost importance since their presence gives rise to optical birefringence and residual porosity. The second phase particles are a source of residual porosity because as the particle continues to dissolve into the matrix by an interdiffusional process, pores located initially inside the particle will eventually be found in the solid solution matrix. Under this condition, pores as large as 30  $\mu\text{m}$  (see Fig. 10) will be found in the sintered material. Pores appreciably larger than 30  $\mu\text{m}$  may be observed if pore coalescence occurs during particle dissolution. The origin of second phase particles in the sintered product is caused probably by the reaction between dried Y-Th nitrate crystals that developed on the upper walls of the beaker containing the oxalic acid solution, and the vigorously stirred oxalic acid solution. Selective precipitation probably occurred during this reaction and yielded Th-rich and Y-rich oxalate agglomerates. The absence of second phase particles in sintered material produced by the standard drip method further supports this reasoning. Numerous dry ball-milling experiments show that regardless of the method used to prepare the oxalate powder, ball milling can completely eliminate solid second phase particles in the sintered material.

### III. ATTEMPTS TO IDENTIFY SUBMICROSCOPIC SCATTERING CENTERS

The substructure (Fig. 5) revealed by the chemical etching technique arises most probably from  $\text{Y}^{3+}/\text{Th}^{4+}$  variations in the resulting microstructure. These fluctuations in composition may originate from chemical differences in the starting powder and from chemical segregation during cooling from the sintering temperature. In the latter case, we shall call these compositional fluctuations extended defects. A critical experiment showed that the laser threshold and the active attenuation coefficient of an NDY laser rod decreased when the rod was fast-cooled instead of slow-cooled from the sintering temperature. This experiment suggested strongly that extended defect formation is occurring during cooling. The  $\text{Y}_2\text{O}_3$ - $\text{ThO}_2$  phase diagram<sup>3</sup> shows that the solubility of  $\text{ThO}_2$  in  $\text{Y}_2\text{O}_3$  decreases from approximately 13 mole % at 2200°C to 6 mole % at 1400°C. Since there is about 10 mole %  $\text{ThO}_2$  in NDY ceramic (neglecting the  $\text{Nd}_2\text{O}_3$  concentration), this solid solution crosses the solvus curve upon cooling from the sintering temperature of 2170°C.

It is conceivable that discrete submicroscopic precipitate particles and/or coherent regions caused by solute clustering may form in the solid solution matrix and represent changes in structure and composition which can produce fluctuations in local refractive index and scatter light. The remainder of this section of the text is devoted to describing experimental results obtained in trying to identify submicroscopic precipitates or other particles, and extended defects, a more general term used to describe Guinier-Preston zones or Wadsley shear structures.

#### A. X-ray Diffraction Results

X-ray diffraction analysis using the diffractometer and Debye-Scherrer techniques was made on NDY powder that was slow-cooled and rapidly cooled from 2170°C to room temperature. The slow-cooled powder was cooled to room temperature in 26 hours, whereas the rapidly cooled specimen was cooled in about 15 minutes. The powders were lightly ground in an agate mortar and pestle and were passed through a -325 mesh nylon screen. Powder diffraction patterns were obtained on these samples using Cu and Cr radiation. Debye-Scherrer lines were somewhat spotty on a dark background caused by Nd fluorescence. An additional grinding treatment helped to eliminate the spotty patterns. There were no unidentified reflection planes observed for the body-centered-cubic lattice of NDY ceramic that was slow- and fast-cooled from 2170°C. A tabulation of d-spacings and relative intensities (peak heights) was made from diffractometer traces. No measurable differences could be detected in line positions; hence, both specimens had approximately the same lattice parameter,  $10.6496 \pm 0.0007 \text{ \AA}$ . A few of the relative intensities were out of line, but this could be due to preferred orientation effects.

Diffractometer traces were obtained at slow speeds ( $0.25^\circ 2\theta/\text{min}$ ) in various parts of the  $2\theta$  range to detect relative amounts of residual strain or clustering effects in both samples. There was no clear evidence of X-ray line broadening caused by strain in either of the large particle size powders. In addition, a low-angle diffractometer scan from  $1^\circ$  to  $8^\circ 2\theta$  showed only a smooth drop to the normal background level. For the slow-cooled sample, this level was reached at about  $2.5^\circ 2\theta$  whereas for the fast-cooled sample, the scattered radiation extended to at least  $3^\circ 2\theta$ .

Although this experimental evidence may be indicative of solute clustering effects, the expected scattering behavior should have been reversed.

It is apparent that X-ray diffraction analysis of slow and fast-cooled powders of NDY ceramic shows very little difference in the unit-cell of both materials. Furthermore, if extended defects (ordered zones) or a metastable transition lattice (metastable precipitate) were formed in the super-saturated solid solution during cooling, large coherency strains that often stabilize these structures should have been detected in the slow-cooled specimen. If coherency strains are present, they are small in magnitude and are difficult to detect with conventional techniques of X-ray diffraction.

#### B. Electron Microscope Results

Slow-cooled and fast-cooled samples of NDY ceramic were examined by direct electron transmission and electron diffraction. The samples were thinned with an ion micromilling instrument in which an ionized Ar beam bombards opposite surfaces of the sample which is rotated. The sample was thinned at a rate of about 1 micron per hour. Samples were coated with a thin conducting layer of carbon and then observed in transmission. Thin chips fractured from large NDY samples were also observed in transmission and diffraction.

A typical electron transmission photomicrograph of NDY ceramic having an average grain size of 150  $\mu\text{m}$  is shown in Fig. 12. The triple point is caused by three intersecting grain boundaries, while the hole is a consequence of complete specimen removal by sputtering. In addition to thickness fringes observed in thin portions of the specimen, there is a mottled structure caused by micromilling because thin chips of the same specimen did not exhibit this mottled appearance. The grain boundaries appeared to be smooth and narrow and free of small second-phase inclusions and substructure. Regardless of whether the specimen was slow or fast-cooled, no substructure could be detected in regions of the specimen far removed from grain boundaries.





Fig. 12 Electron transmission photomicrograph of grain boundaries in NiDY ceramic  
thinned by ion micromilling. 48,000X

Selected area diffraction (SAD) photomicrographs were obtained from various regions within a given grain. Reciprocal lattice patterns, which could be indexed on the large b.c.c. lattice cell, did not appear to be obviously different from one region to another. Perhaps a more extensive investigation using SAD should be made on NDY ceramic cooled at different rates or isothermally aged at low temperatures.


### C. Ultramicroscopy

An ultramicroscope is an optical arrangement in which a very intense beam of light is directed onto the object at right angles to the microscope optical axis. By making use of scattered light, it is possible to observe particles well below the resolving power of the microscope. It is generally believed that particles as small as  $0.005 \mu\text{m}$  can be observed but not exactly measured with ultramicroscopy if properly employed.<sup>4</sup>

The number of scattering centers, such as pores less than  $0.5 \mu\text{m}$  in size, were determined in a given solid volume with the help of ultramicroscopy. Here the sintered NDY rod, having a polished flat parallel to the longitudinal axis of the rod, was illuminated by an intense beam of He-Ne laser light (1 mW output,  $\lambda = 6328\text{\AA}$ ) at  $90^\circ$  to the microscope optical axis. A typical photomicrograph taken at a low magnification (X10) is shown in Fig. 13. Distinct scattering centers and a visible background haze are evident. By focusing the microscope through the polished flat, second-phase particles appeared as bright spots of scattered light against a nearly dark field. The total number density of distinct microscopic and submicroscopic scattering centers was determined by counting bright spots while scanning through a known solid volume at a magnification of X460. The number density of distinct submicroscopic scattering centers in the rod was calculated by subtracting the number density of microscopic pores ( $\geq 0.5 \mu\text{m}$  in size) measured by transmitted-light microscopy from the total number density of distinct scattering centers measured by ultramicroscopy. It was found that only about 20% of the total number of observed scattering centers were smaller than  $0.5 \mu\text{m}$  in size.



Fig. 13 Ultramicroscope photomicrograph of scattering centers in a NDY ceramic rod. 10X

Reproduced from  
best available copy. 

The material loss (attenuation) coefficient determined by active (lasing) measurements was found to be approximately  $5.4\% \text{ cm}^{-1}$  for the NDY rod examined by ultramicroscopy. Scattering appeared to be the mechanism responsible for most of this optical attenuation because when an He-Ne laser beam passed through the rod, the path of light was clearly visible on all sides and, as a result, the rod appeared bright in a dark background. If it is assumed that absorption effects are much smaller than scattering effects and that pores are the major scattering centers, then the attenuation coefficient in the solid medium at the lasing wavelength can be calculated from light scattering theory assuming spherical, nonabsorbing pores which act as single scattering centers. Scattering losses per unit length ( $-\frac{dI}{I dz}$ ) can be described by

$$-\frac{dI}{I dz} = \gamma = \sum_i n_i C_i \quad (1)$$

where  $I$  = beam intensity (joules/sec.  $\text{cm}^2$ ) at a given value of  $z$  and wavelength,  $\gamma$  is the active attenuation coefficient,  $n_i$  = number density of pores in a given size range ( $i$ ) and  $C_i$  = the total scattering cross section over that size range. By using theoretical equations<sup>5</sup> of  $C_i$  for pores both small and large compared to the wavelength of light in the NDY laser rod; i.e.,  $\lambda = 5,680 \text{ \AA}$ , hypothetical plots of  $\log C_i$  versus  $\log d_i$ , where  $d_i$  is the average pore size over the size range ( $i$ ), showed that pores greater than about  $0.3 \text{ \mu m}$  followed scattering behavior expected for large particles. This means that for  $d_i > 0.3 \text{ \mu m}$ ,  $C_i$  is simply equal to twice the geometric cross section.<sup>5</sup> An error of about 10% is introduced if 2 is taken as the scattering efficiency factor. Under the above assumptions, and using Equation 1, a theoretical  $\gamma$ -value of about  $0.22\% \text{ cm}^{-1}$  was calculated for the pore size distribution observed microscopically in the laser rod. The calculated value of  $\gamma$  was approximately a factor of 25 lower than the experimentally determined value of  $5.4\% \text{ cm}^{-1}$ .

The experiment using microscopy showed that only about 20% of the total number of scattering centers observed were smaller than  $0.5 \text{ \mu m}$  in size, and such a small number of submicroscopic pores or solid second phase particles cannot account for the attenuation coefficient measured

experimentally. In addition to the presence of distinct submicroscopic scattering centers observed as points of light under the ultramicroscope, a background haze was visible in the beam path traversing the specimen and suggested that the scattered light is weak and may be caused by submicroscopic scattering centers having a refractive index which is not very different from that of the matrix. If the visible haze is indeed real, then the origin of submicroscopic scattering centers in NDY ceramics may be caused by orange peel and extended defects. The scattering of light by grain boundaries in optically isotropic NDY ceramics is predicted to be almost negligible compared to other scattering effects because a grain boundary free of gross segregation and a solid second phase has a very small scattering cross-section due to its small width compared to the lasing wavelength and its small difference in refractive index from that of the grain interior. In addition, these NDY ceramics have large grain sizes ( $>130 \mu\text{m}$ ) which give rise to small grain boundary volume available for scattering.

It is emphasized that if the assumptions introduced above are valid, then  $\text{ThO}_2$ -doped  $\text{Y}_2\text{O}_3$  represents a polycrystalline laser host in which porosity is no longer the major scattering defect when the residual porosity is equal to or less than  $10^{-6}$ . The principal cause of light scattering in NDY ceramics is related to the presence of unidentified submicroscopic scattering centers having a refractive index which differs little from that of the matrix. The separation of absorption and scattering losses from the total optical loss can shed more light on these experimental and theoretical results and is currently under investigation.

#### IV. OPTICAL MEASUREMENTS

##### A. Lasing Measurements

Recently, it was discovered<sup>1</sup> that the cooling cycle influences the optical quality and, therefore, the lasing performance of an NDY ceramic rod. There was a large improvement in the lasing performance by fast-cooling, rather than by slow-cooling the same rod from the sintering temperature. In order to see if reproducibility could be achieved, a second NDY rod was given the following heat treatment. First, the rod was slow-cooled

from 2170°C to about 800°C in 5.5 hours. After measuring the lasing threshold, active loss coefficient and lasing slope efficiency, the same rod was heated to 2170°C for two hours to equilibrate the sample and then cooled rapidly to about 800°C in one hour. Below 800°C, no structural changes are thought to occur because ionic mobilities are probably very small.

A comparison of the lasing data obtained for the slow-cooled (12-1B) and fast-cooled (12-1A) NDY rod is shown in Figs. 14 and 15. The laser threshold value using a 95% reflectivity output mirror is 21 joules for the slow-cooled specimen and 17 joules for the fast-cooled specimen. By plotting  $\frac{1}{R_1 R_2}$  as a function of threshold energy on a semilogarithmic scale (Fig. 14) and extrapolating to zero pump energy or threshold energy, the intercept along the ordinate gives

$$\ln \frac{1}{R_1 R_2} = -\gamma 2l \quad (2)$$

where  $R_1$  and  $R_2$  are the mirror reflectivities. The active attenuation coefficients for the slow-cooled and fast-cooled NDY rod were 5.4%  $\text{cm}^{-1}$  and 4.5%  $\text{cm}^{-1}$ , respectively. Laser output using laser glass as a reference material, was measured as a function of input energy (Fig. 15). The NDY rod was smaller in diameter than the glass rod and, consequently, the data plotted in Fig. 15 were normalized with respect to the diameter of the glass rod because large rod diameters give rise to increased surface area available for capturing of flashlamp radiation. The lasing slope efficiencies for a rod that was slow-cooled and fast-cooled from the sintering temperature were 0.10% and 0.16%, respectively. These lasing measurements show that an NDY laser rod has an improved lasing performance by a fast-cooling treatment from the sintering temperature. However, there is a limit to how fast an NDY rod can be cooled without specimen fracture caused by thermal stresses. It is believed that the rapid cooling treatment helps to retain the high-temperature, disordered solid solution and retards nucleation and growth of extended defects at lower temperatures.

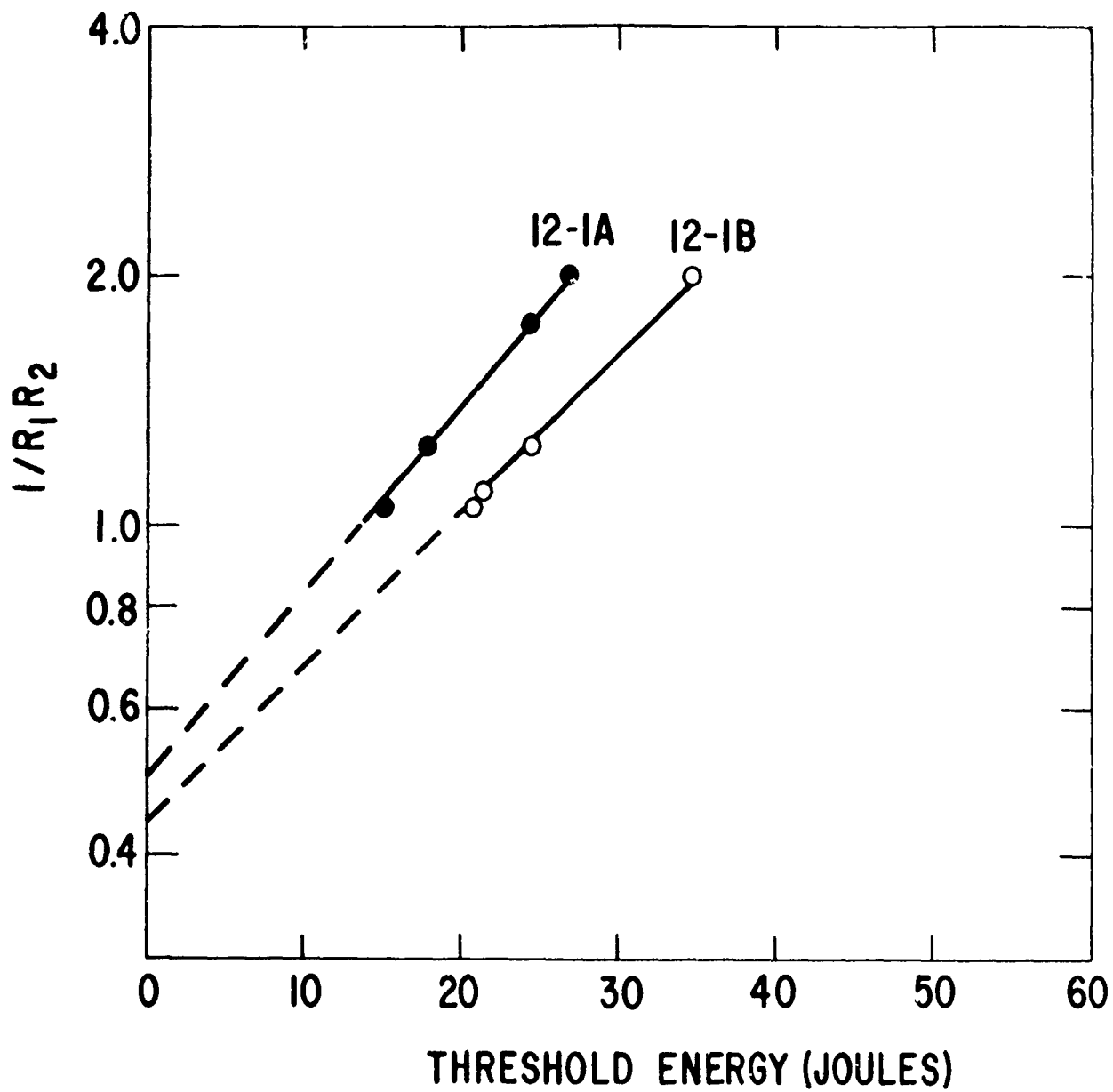


Fig. 14 Effect of output mirror reflectivity ( $R_2$ ) on the pump energy required for laser threshold. Same rod that was fast-cooled (12-1A) and slow-cooled (12-1B) from the sintering temperature of  $2170^\circ\text{C}$ .  $R_1 \approx 1$

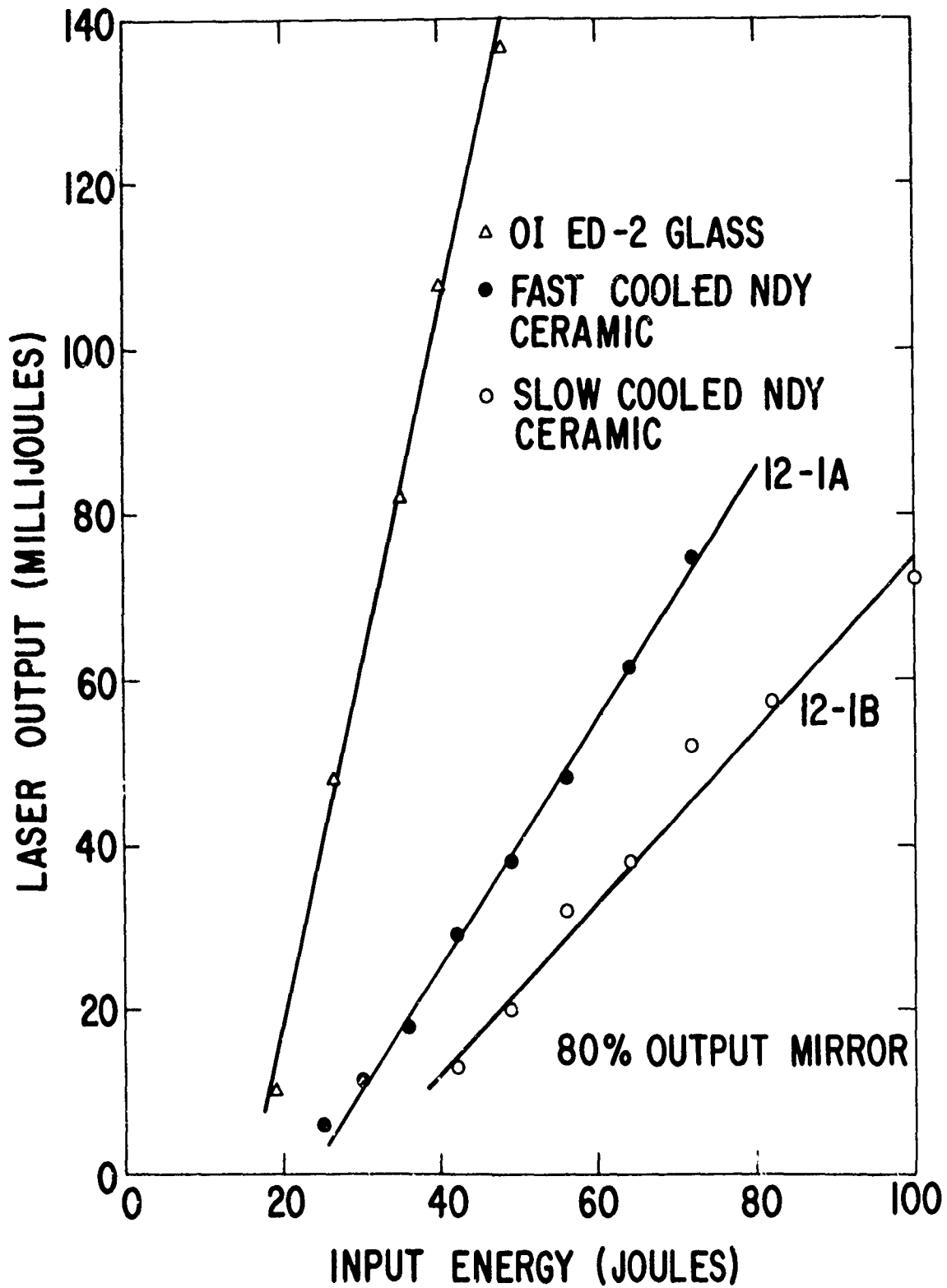


Fig. 15 Energy output versus energy input for the same rod that was fast-cooled (12-1A) and slow-cooled (12-1B) from the sintering temperature of 2170°C, laser glass (OI - ED-2) was used as a reference material.



Laser threshold measurements can determine readily the degree of optical perfection displayed by a given laser rod. In this way, the influence of powder preparation and processing on the optical quality of a sintered rod can be measured and evaluated. A laser rod was produced by the aerosol technique of powder preparation combined with dry-milling the oxalate powder to see if NDY ceramic could be made with an improved laser performance. The lasing threshold was determined to be 21.6 joules at 95%  $R_2$  (output mirror reflectivity) and was essentially the same as that determined for 12-1B rod which was made by a combination of the drip method and dry-milling the calcined oxides before sintering. It is concluded that it is very difficult to drastically improve the lasing behavior of NDY ceramic by using the oxalate approach combined with a milling operation.

#### B. Laser Damage Threshold

A true measure of the lasing capabilities of Nd-doped Yttralox ceramic is to compare its lasing performance to that of glass:Nd under Q-switching conditions. Under normal-mode lasing conditions, the best NDY laser rod has a lasing slope efficiency 43% that of a glass:Nd rod. In Q-switching operations, however, NDY lasers may achieve higher average power output than glass:Nd lasers because the thermal conductivity of NDY ceramic is about five times higher.

Laser damage threshold tests on NDY rods have been initiated recently, and these results will be reported in the next technical summary. Laser rods will be tested for laser damage with the help of Q-switching techniques. In order to detect laser damage threshold, the energy will be increased slowly until damage sites can be detected by optical methods.

Preliminary lasing results show that for the laser cavity employed, it is necessary to use an RTV seal between the Schott yellow filter glass and the pump cavity to eliminate discoloration of the NDY rods. Discoloration or radiation darkening is caused by the absorption of ultraviolet radiation from the flashlamp output. If discoloration did occur, a low-temperature anneal at 250 to 300°C was able to clear the rod.

### C. Influence of Stoichiometry on Transparency of Yttralox

The development of polycrystalline NDY ceramics with high optical quality has been previously shown to depend on improved powder preparation and processing techniques and on controlled porosity, grain size, impurities, and variation in chemical composition in the sintered material. An additional requirement has been shown recently to be controlled stoichiometry. Controlled oxidation of neodymium-free Yttralox ceramic at high temperatures can generate a pronounced middle infrared pass filter or a visible-to-middle infrared pass filter.

Spectral transmittance of Yttralox ceramic (90 mole %  $Y_2O_3$  + 10%  $ThO_2$ ) sintered in wet  $H_2$  ( $P_{O_2} \approx 10^{-8}$  atm) and in dry  $H_2$  ( $P_{O_2} \approx 10^{-15}$  atm) at 2170°C were measured with Cary Model 14 and Perkin-Elmer Model 521 spectrophotometers. For a 1 mm thick plate, the short and long wavelength cutoffs are 0.25 and 9.5  $\mu m$  for material fired in wet  $H_2$  and 1 and 8  $\mu m$  for material fired in dry  $H_2$  at 2170°C. The color of Yttralox fired in wet  $H_2$  is water-white, whereas that of material fired in dry  $H_2$  is black. Both clear and black materials are cubic single phases, as ascertained by X-ray diffraction analyses using the Debye Scherrer method, and have lattice parameters of  $10.6496 \pm 0.0007 \text{ \AA}$  and  $10.6476 \pm 0.0005 \text{ \AA}$ , respectively. The black color and smaller unit-cell associated with this yttria base solid solution fired in low  $P_{O_2}$  atmospheres are related probably to the removal of a considerable number of oxygen ions from the lattice, causing possible F-center formation in which oxygen vacancies trap electrons.

### V. REFERENCES

1. C. Greskovich, "Oxide Ceramic Laser", Annual Report, July 1972.
2. C. Greskovich and K. N. Woods, "The Fabrication of Transparent  $ThO_2$ -Doped  $Y_2O_3$ ", accepted by the Bull. Amer. Ceramic Society, October 1972.
3. E. C. Subbarao, P. H. Sutter, and J. Hriza, "Defect Structures and Electrical Conductivity of  $ThO_2$ - $Y_2O_3$  Solid Solutions," J. Amer. Ceram. Soc., 48 (9) 443-46, (1965).

4. C. P. Schillaber, Photomicrography in Theory and Practice, J. Wiley and Sons, Inc., New York, pg. 741 (1947).
5. Van De Hulst, Light Scattering By Small Particles, John Wiley and Sons, Inc., New York, pp. 64 and 107 (1957).